Published in final edited form as:
J Mol Biol. 2009 March 6; 386(4): 1038–1053. doi:10.1016/j.jmb.2009.01.003.

Structural basis for catalysis of a tetrameric, class IIa *fructose* 1,6-bisphosphate aldolase from *M. tuberculosis*

Scott D. Pegan[1], **Kamolchanok Rukseree**[2,3], **Scott G. Franzblau**[2], and **Andrew D. Mesecar**[1,2]

1 *Department of Medicinal Chemistry and Pharmacognosy and the Center for Pharmaceutical Biotechnology, the University of Illinois at Chicago, 60607*

2 *Institute for Tuberculosis Research, the University of Illinois at Chicago, 60612*

3 *National Center for Genetic Engineering and Biotechnology (BIOTEC), NSTDA, Thailand Science Park, 12120*

Abstract

Mycobacterium tuberculosis, the causative agent of tuberculosis (TB), currently infects one third of the world's population in its latent form. The emergence of multidrug resistant strains, MDR-TB and XDR-TB has highlighted the need for new pharmacological targets within *M. tuberculosis*. The Class IIa fructose 1,6-bisphosphate aldolase (FBA) enzyme from *M. tuberculosis* (MtFBA) has been proposed as one such target since its upregulated in latent TB. Since the structure of MtFBA had not been determined and since there was little information available on its reaction mechanism, we sought to determine the X-ray structure of MtFBA in complex with its substrates. By lowering the pH of the enzyme in the crystalline state, we were able to determine a series of high-resolution X-ray structures of MtFBA bound to dihydroxyacetonephosphate (DHAP), glyceraldehyde-3-phosphate (G3P), and fructose 1,6-bisphosphate (FBP) at 1.5 Å, 2.1 Å, and 1.3 Å respectively. Through these structures it was discovered that MtFBA belongs to a novel tetrameric class of the type IIa FBAs. The molecular details at the interface of the tetramer revealed important information for being able to better predict the quaternary structures among the FBAs based on their primary sequences. These X-ray structures also provide interesting and new details on the reaction mechanism of class II FBAs. Not only were the substrates and products observed in geometries poised for catalysis, but unexpectedly the hydroxyl enolate intermediate of DHAP was also captured and resolved structurally. These concise new details provide a better understanding of the reaction mechanisms for FBAs in general and provide a structural basis for inhibitor design efforts aimed at this class of enzymes.

Keywords

class II fructose-1,6-bisphosphate aldolase; zinc enzyme; mechanism; Mycobacterium tuberculosis; dihydroxyacetone; glyceraldehyde-3-phosphate; aldol condensation

*Address correspondence to Andrew D. Mesecar, Center for Pharmaceutical Biotechnology, the University of Illinois at Chicago, 900 S. Ashland, M/C 870, Chicago, IL 60607. Phone (312) 996-1877; Email; mesecar@uic.edu.

Accession Codes:
Structure factors and coordinates have been deposited with the Protein Data Bank and assigned codes 3EKL, 3EKZ, 3ELF.

Introduction

Tuberculosis (TB) is one of the most prevalent infections in the world and a leader among the causes of mortality in developing countries. Infections by *Mycobacterium tuberculosis*, the causative agent for TB, have been estimated by the World Health Organization (WHO) at 9.2 million new cases during 2006 with 1.7 million *M. tuberculosis* related deaths. This is an increase over the 9.1 million new cases reported in 2005[1]. Additionally, one third of the worlds population is estimated to have latent *M. tuberculosis*[1]. Although the increase in new TB cases is attributed to the population growth, new drug-resistant strains have also emerged that threaten to increase this number and thwart efforts to eradicate this disease. Incidences of multidrug-resistant TB (MDR-TB) and extensive drug resistant TB (XDR-TB) are on the rise, requiring the development of new treatment regiments, drugs, and drug targets[2].

One potential drug target for TB is *M. tuberculosis* fructose 1,6-bisphosphate aldolase class II (MtFBA; E.C. 4.1.2.13). MtFBA is one of two classes of fructose 1,6-bisphosphate aldolases (FBA) located within *M. tuberculosis*. These FBAs are responsible for mediating the second reversible step of the glycolytic pathway, which supplies glyceraldehyde 3-phosphate (G3P) for downstream enzymes in the pathway and fructose 1,6-bisphosphate (FBP) for gluconeogenisis. Together, the substrates and products of the FBA reaction are crucial for the supply of these precursor molecules to other biochemical pathways essential for the survival of *M. tuberculosis*.

Class I and Class II FBAs both catalyze the reversible adol condensation of dihydroxyacetone phosphate (DHAP) with G3P to form fructose 1,6-bisphosphate (FBP)[3], and both classes are hypothesized to have evolved independently from a common ancestor since they are both composed of $(\alpha/\beta)_8$ barrel folds[4]. However, the two classes differ in the mechanisms they utilize to catalyze the reaction, their prevalence among species, and their roles in autotrophic prokaryotes. For instance, although both aldolases form enolate anions from DHAP for their reaction with G3P, Class I FBAs use the ε-amino group of a lysine to elicit a Schiff-base intermediate, whereas Class II aldolases utilize a Zn(II) cation to stabilize the enolate intermediate. Class II FBAs are also activated by monovalent cations such as Na(I)[3].

In addition to the differences in their reaction mechanisms, the two classes of FBAs also differ in their distribution among different species. Higher organisms possess only Class I FBAs, whereas protozoa, bacteria, fungi, and blue-green algae primarily have Class II FBAs with a few possessing both[5; 6; 7]. In those species where both classes of FBAs are present, such as in *E. coli* and other autotrophic prokaryotes, only the class II FBA genes appear to be essential[4; 8; 9]. Single gene knockout attempts of the *E. coli* fbaA gene (class II) have proven to be unsuccessful whereas knockouts of the fbaB gene (class 1) are viable[8; 10]. Significant expression levels of class I FBA in *E. coli* were only observed in the presence of gluconeogenic substrates, suggesting class I FBAs are only conditionally present[11]. An *E. coli* strain, JM2087, with 11 gene mutations including the fbaA-1 gene has been reported to be viable but the precise reason for the viability and the nature of the mutation in the fbaA-1 gene are ambiguous[12]. The studies on the *E. coli* fba genes are consistent with studies on *M. tuberculosis* where only the class I enzyme is observed during high aeration conditions, while under hypoxic conditions, the class II MtFBA is singularly expressed at high levels[13; 14]. Attempts to replace the wild-type fba (class II) gene in *M. tuberculosis* with a deleted allele (Δfba) by a two-step homologous recombination procedure have also proven unsuccessful[15].

Since one of the difficulties in the successful treatment of *M. tuberculosis* infections is the bacteria's ability to adopt a latent phenotype that allows survival of the bacterium under hypoxic conditions, targeting enzymes that are essential for survival under these conditions is vital. The lack of a class II FBA in humans and its critical role in the bacteria highlight MtFBA

as a promising target for pharmaceutical development[16]. Previous efforts to design inhibitors for class II FBAs have had limited success due to lack of robust selectivity for class II FBAs over class I FBAs[17; 18]. Efforts to further develop these and other new inhibitors through structure-based drug discovery (SBDD) efforts have been hindered by the lack of available MtFBA structures. Moreover, structures of any class II FBA in the productive substrate-bound, intermediate-bound, or product-bound complexes are currently unavailable.

Class II FBAs can be further categorized into class IIa and class IIb families. Traditionally, class IIa and class IIb FBAs were categorized according to sequence homology and their oligomeric state. Class IIa FBAs were considered dimers, while class IIb FBAs could be either dimers, tetramers, or octomers[5; 6; 19] Members belonging to each family are observed to exhibit 40% sequence similarity with 25–30% sequence similarity to all class II FBAs[20]. MtFBA has been traditionally classified as a class IIa FBA based on its significant sequence homology to other class IIa FBAs (*E. coli* and *Streptomyces galbus*; Figure 1) [20; 21]. However, during recent expression studies on MtFBA, the enzyme was observed to form a tetramer during analytical size-exclusion chromatography even though it is considered to be a member of the class IIa FBAs[4].

Structures have been determined for members of each family and these structures have been assumed to be representative of each family in general. Structures of class IIa and IIb FBAs in complex with the inhibitor phosphoglycolohydroxamate (PGH), have been determined[6; 21]. Although PGH and its analogs are potent inhibitors of FBAs due to their structural similarity to DHAP, this similarity also makes them potent inhibitors of the human class I FBAs which makes them non-specific and undesirable for drug development[17]. Additionally, the available X-ray structures of PGH complexes only provide general insight into one reaction step in the class II FBA mechanism thereby leaving all of the other steps of reaction unexplored structurally. A more thorough understanding of the structural basis for the binding and catalysis of substrates and products by MtFBA would therefore significantly enhance our understanding of the overall catalytic mechanism of Class II FBAs as well as provide a better rationale for the development and improvement of existing and new class II FBA inhibitors.

To investigate the oligomeric nature of this unique member of the class IIa FBAs and to aid in future SBDD efforts, an in depth, X-ray structural characterization of MtFBA was conducted with its natural substrates & products. X-ray structures of MtFBA in complex with DHAP, G3P, and FBP were determined to high resolution and reveal that MtFBA belongs to a novel, tetrameric class of the type IIa FBAs. The molecular details at the interface of the tetramer provide important information for better predictability of the oligomeric states among the FBAs based upon their primary sequences. The structures also provide interesting and new details on the reaction mechanism of class II FBAs. Not only were the substrates and products observed in geometries poised for catalysis, but unexpectedly the hydroxyl enolate intermediate of DHAP was also captured and resolved structurally.

Results

X-ray structural elucidation of MtFBA

A series of X-ray structures of MtFBA in complex with G3P, DHAP, and FBP were determined to resolutions between 1.3 Å and 2.1 Å (Table 1). The construct of MtFBA used for crystallization contained the full length MtFBA enzyme with five additional histidine residues added to the C-terminal histidine forming a hexahistidine affinity tag. MtFBA was co-crystallized with the substrate DHAP, and the complex crystallized as a monomer in the asymmetric unit (Figures 2a and 2b). One sodium and two zinc cations were found bound to each monomer (Figures 2 and 3). One of the two zinc cations (Zn1) is located within the active site whereas the other zinc atom (Zn2) is located at a crystal contact between two symmetry-

related MtFBA monomers formed through coordination to the hexahistidine tag (not shown). Specifically, Zn2 coordinates, with the δ-nitrogen of H344, the ε-nitrogen of H346 and the oxygen atom of water 105. Fourth and fifth coordination positions are occupied by the carboxyl group of E198 and ε-nitrogen of H199 of a symmetry related MtFBA monomer.

The secondary structure of MtFBA resembles that of other bacterial class II aldolases [5; 22] (Figures 2a and b). MtFBA has an eight stranded β-sheet core where each β-strand (β1– β8) is followed in general by an α-helix (α1– α8a) giving rise to an overall $(\beta/\alpha)_8$-barrel fold. There are two deviations to the typical $(\beta/\alpha)_8$ barrel fold in MtFBA; one is the presence of a previously unobserved 3_{10}-helix between β-strand β3 and α-helix α3, and the other is an extra α-helix, α2a, between α-helix α2 and β-strand β3 (Figure 1). In addition to the $(\beta/\alpha)_8$-barrel, four helices are also present within a monomer. One of these helices, α0, blocks the entrance to the $(\beta/\alpha)_8$-barrel on its N-terminal side (Figure 2a). Two other helices, α8b and α8c which are not observed in other FBA structures, form at the apex of an arm formed by α8 and the fourth additional helix, α8a(Figure 2a). This arm, and the $(\beta/\alpha)_8$-barrel fold, result in a monomer with dimensions of 78 Å, 52 Å, and 40 Å.

Quaternary Structure and T-Region of MtFBA

The quaternary structure of MtFBA in solution is consistent with it being a tetramer based upon our analytical, size-exclusion chromatography experiments and those reported previously.[4]. Therefore, the monomer observed in the asymmetric unit is likely only the protomer of a larger, symmetrical tetramer. Analysis of the symmetry related monomers within the unit cell of the I222 space group suggests that MtFBA exists as a dimer-of-dimers with D2 quaternary symmetry consistent with the tetrameric species observed from size-exclusion chromatrography. The monomer-monomer interface of the dimer has a total contact suface area of 2617 $Å^2$. This value compares well with the expected ranges of subunit, interfacial surface areas for proteins with similar subunit molecular weights[23]. The monomer-monomer interactions within the dimer are facilitated by a mix of H-bonds, salt bridges, and hydrophobic packing which are also observed at the interface of the dimeric *E. coli* FBA[22]. In summary, the monomer-monomer interface of the dimer is facilitated by the packing of α2a against its symmetry related self and α8, α8a, α8b on the arm of the monomer crossing over its symmetry related counter part (Figure 2c).

The dimer-of-dimers interface of the tetramer involves a total contact surface area of 1220 $Å^2$ which is somewhat less than a value of ~2,500 to 3,600 $Å^2$ which is a general range for tetramers with similar molecular weights[23]. There are, however, a number of major interactions between the two dimers formed from a series of residues spanning from Y281 on the α8a helix, to D302 just slightly beyond helix α8b. This region is designated the tetramerization region or 'T-region' (Figure 1› 2b,c,d) [24]. The T-region mediates tetramer formation by its interactions with other, symmetry related T-regions (Figure 2c). At the core of this interaction are residues F292 and Y295 which form interdimer, hydrophobic interactions. Another set of hydrophobic interactions located at the T-region interface are observed between L299 and V301. In addition to hydrophobic interactions, the side-chain hydroxyl group of Y295 also forms an H-bond with the side chain of R285. The side chain of R285 also participates in an H-bond network with the side chains of Y281 and D302. There is also an interdimer, main-chain interaction formed by the amide of K300 and carbonyl of D302 from different dimers (Figure 2d).

MtFBA-DHAP bound Active Site

Examination of F_o-F_c electron density difference maps within the active site of the MtFBA-DHAP complex revealed strong, residual density not only for the substrate, DHAP, but remarkably, also for its hydroxyl-enolate intermediate (HEI). Under normal solvent conditions

in the absence of enzyme, the C1 atom of DHAP is in an sp^3 hybridized orbital with tetrahedral geometry. However, when bound to the active site, the bulk of the electron density associated with DHAP in the active site surrounding the C1–C2 bond of DHAP is planar suggesting that the C1 atom is mainly in an sp^2 hybridized orbital consistent with a double bond between C1=C2. This observation lends support for an HEI-like intermediate being bound within the active site. The geometry at the C1 position is similar to that of the FBA inhibitor phosphoglycolohydroxamate (PGH). Modeling and refinement of an HEI molecule within the electron density accounted for the bulk of the electron density within the difference maps (Figure 3a). However, a significant peak (> 3σ in the F_o-F_c difference maps still remained and was only fully accounted for when the substrate DHAP was modeled into the density and refined at an occupancy ratio of 30:70 DHAP to HEI (Figure 3a,b). Finally, the average B-factor of 20.6 $Å^2$ for the ligands is near the average value of 19.8 $Å^2$ for the protein (Table 1).

The active site of the HEI/DHAP bound form of MtFBA closely resembles those of other bacterial class II aldolase structures bound with the inhibitor PGH[6; 25]. For HEI, both the C1 hydroxyl and C2 enolate-oxygen coordinate directly to the catalytic zinc, Zn1, which is coordinated directly to the enzyme by three histidines, H96, H212, and H256. As a result, the coordination number of ZN1 is 5 (T_5) and its geometry is that of a non-ideal, trigonal bipyramid[26]. The C1 hydroxyl of HEI also forms an H-bond with D95 (2.5 Å), while the C2 enolate-oxygen forms an H-bond interaction with the backbone amide group of G253 (3.0 Å) (Figure 3c). Similar to HEI, the C2 ketone oxygen of DHAP forms an H-bond with the backbone amide of G253 and it also coordinates to Zn1 with a bond distance of 2.6 Å which is a bit longer than the bond distance between the enolate oxygen of HEI and Zn1 which is 2.2 Å. The C1 hydroxyl group of DHAP forms H-bond interactions with the side chain of D295 (3.0Å) and with nearby active site waters (Figure 3d). The remaining MtFBA-HEI/DHAP interactions are indistinguishable between each other. The phosphate group of both the HEI and DHAP form H-bonds with the side-chain hydroxyl and backbone amide groups of S255 and T277, as well as an ionic interaction with the Na+ (Figure 3d).

MtFBA-G3P-DHAP pre-catalysis structure

MtFBA is observed to have a sharp pH optimum of 7.8[4]. Above or below this pH, MtFBA quickly loses its ability to mediate the enol condensation of DHAP and G3P or its reversible reaction[4; 7]. The crystallization conditions of MtFBA-DHAP involved preincubation of the enzyme with the substrate DHAP with buffering at pH ~8, and then setting up crystallization trials with buffering at pH 4.8. The drop in pH upon crystallization suggests that we have trapped MtFBA with DHAP and an HEI-like intermediate bound in a catalytically unreactive form. In the case of HEI, this may actually result in the formation of an enediol intermediate (see Discussion).

We took advantage of this low pH trapping approach and soaked MtFBA-DHAP/HEI crystals for 24 hrs in mother liquor containing 2 mM of the substrate G3P prior to X-ray data collection. A complete X-ray data set of 2.1 Å was obtained and refined against the MtFBA-DHAP/HEI structure (Table 1). Overall, the tertiary structure of MtFBA remained unchanged. However, additional and strong (>3σ electron density in F_o-F_c difference maps was observed within the active site (Figure 4a). Examination of both F_o-F_c and $2F_o$-F_c weighted maps proved the density to be that for G3P and DHAP/HEI and not for fructose 1,6-biphosphate (Figure 4a,b). Thus, we effectively trapped the Michaelis complex for the MtFBA catalyzed reaction. Final refinement of the structure with HEI/DHAP and G3P resulted in R_{work} and R_{free} values of 15.8% and 18.1% respectively.

Within the active site of the MtFBA-G3P-DHAP/HEI structure, the position of the HEI molecule remained unchanged, compared to the DHAP/HEI complex, but the DHAP molecule was pushed slightly deeper into the active site pocket with the C1 hydroxyl group rotating away

from the water molecule it had previously formed an H-bond with (Figure 4). In the end, this placed the C1 of DHAP about 4.4 Å from the C1 of G3P in comparison to the distance of 3.3 Å between the C1 of HEI and C1 of G3P (Figure 4c). In comparison to the DHAP/HEI binding site that used cations and backbone amide groups, G3P binding is facilitated mostly through interactions with side chains and water molecules (Figure 4c). Specifically, the C2 hydroxyl of G3P forms H-bonds with active site waters that are also shared with the DHAP binding site. This hydroxyl also forms a direct H-bonds (3.0 Å) with the side chain of D276 that also forms a weak H-bond (3.4 Å) with the phosphoester oxygen as well as H-bonds with water molecules directly hydrogen bonded to the phosphate moiety.

The C6-phosphate moiety is G3P's main source of interaction with MtFBA. The phosphate oxygens form H-bonds with the side chain of S53 and with the side chain guanidinium group of R314 from a symmetry related monomer at the dimer interface. The remaining H-bonds are formed with waters and the side chains of K308 and R314 which are contributed by symmetry related monomers. The importance of the interaction between R314 and the C6-phosphate of FBP and G3P has been shown through mutagenesis and modeling experiments with *E. coli* FBA[27; 28]. When the equivalent residue (R331) in *E. coli* is mutated to an alanine residue, a 26-fold increase in the K_M value for FBP and a 29-fold decrease in k_{cat} are observed [27].

MtFBA-FBP structure

Since the interaction of FBA with the substrate FBP has not been reported for any Class II or bacterial aldolase, it was therefore of great interest to determine. We first attempted to co-crystallize FBP with MtFBA which produced crystals suitable for X-ray diffraction. We collected a 1.7 Å dataset and refined the model against the MtFBA-DHAP structure with DHAP removed. Unfortunately, only density supporting the presence of DHAP/HEI was observed indicating that FBP had undergone complete cleavage. Evidently, the resulting steady-state concentration of G3P was insufficient to adequately occupy the G3P site (Figure 1S). Cleavage of the FBP in these drops was not a complete surprise since FBP was added directly to the protein solution buffered at pH 8 prior to conducting crystallization trials.

To overcome this issue, we took advantage of the low pH conditions of the preformed MtFBA-HEI/DHAP crystals and attempted to trap FBP in the active site by soaking the crystals overnight in mother liqueur containing 10 mM FBP. A 1.3 Å X-ray data set was collected and the data were refined against the MtFBA-DHAP structure with ligands removed. Under these conditions, strong (>3σ and continuous electron density was apparent in F_o-F_c and $2F_o$-F_c difference maps which was consistent with a fully occupied FBP molecule (Figure 5A). The average B-factor value of 17.2 $Å^2$ for the ligands was also found to be slightly lower than the average value of 18.4 $Å^2$ for the protein (Table 1). Thus, under the experimental conditions employed, the bound DHAP and HEI molecules were able to exchange with free FBP from solvent.

The active site structure of the MtFBA-FBP structure was remarkably similar to the other two complexes in that the residues, ions, and waters forming interactions between the enzyme and FBP are similar to those involved in binding DHAP/HEI and G3P (Figure 5). The C1 phosphate moiety of FBP is bound by the same residues and sodium ion as observed for DHAP/HEI and DHAP/G3P (Figures 5a and b). The C3 hydroxyl oxygen coordinates with the catalytic zinc with a short bond distance of 2.2 Å whereas the C2 ketone and C4 hydroxyl groups coordinate with the zinc with slightly longer bonds of 2.6 Å and 2.4 Å respectively. In addition to coordinating to Zn1, the C4 hydroxyl group, which would be deprotonated during the cleavage of FBP in the glycolytic direction, forms an H-bond interaction with an active site water (2.7 Å) and it comes in close proximity to D276 (3.7 Å) which is proposed to accept the proton from the C4 hydroxyl.

Discussion

Modes of tetramerization among class II FBAs

The structure of MtFBA highlights the structural divergence of tetramer formation between class IIa and IIb FBAs. Similar to class IIa MtFBA, *T. aquaticus* FBA forms a tetramer through a dimer-dimer interaction. However, the dimer-dimer interaction in *T. aquaticus* FBA is formed along helices α3 and α4 whereas in MtFBA the tetramer interface lies on the other side of the dimer along α8a and the previously unobserved single helical turn, α8c. The preference for one form of tetramerization over the other can be deciphered from the sequences and structural comparison of the MtFBA and *T. aquaticus* FBA. MtFBA, as with other class II FBAs, possesses a conserved insert of 10 residues (98–108) comprising a 3_{10} helix, and a four residue insertion (121–124) which accommodates the 3_{10} helix (Figure 1, 2b). These additional residues of MtFBA and other class IIa FBAs create a steric clash if packed in the same manner of the *T. aquaticus* tetramer. Thus, the *T. aquaticus*-like tetramer cannot form.

Just as structural features of MtFBA inhibit tetramer formation in the manner of *T. aquaticus*, the lack of structural features in *T. aquaticus* in the tetramerization domain of MtFBA inhibits *T. aquaticus* FBA from forming tetramers like MtFBA. *T. aquaticus* FBA does not possess an insertion of 13–18 residues in length (MtFBA 294–306) that is present in the majority of class IIa FBAs, MtFBA (*E. coli* FBA and *S. galbus* FBA; Figure 1). These 13 residues in MtFBA form a significant part of the T-region and form five hydrophobic and two ionic interactions essential to tetramer formation (Figure 2b,d). Interestingly, the presence of an insert at the T-region location does not automatically infer tetrameric assembly among class IIa FBAs. *E. coli* FBA contains an insert at this location but is a dimer leading to the conclusion that certain key sequence positions must contain specific amino acids in order to produce a tetrameric species. With the nature of MtFBA and *T. aquaticus* FBA's tetrameric assembly now known, the potential of predicting other class IIa and IIb FBA tetramers can be realized.

Divergent methods of oligomerization among isoenzymes have been reported for other enzymes. Glutamate racemase 1 and 2 have been observed to adopt different dimer-dimer interactions despite high sequence similiarity[29]. Both class I and class II FBAs have been observed to form multiple oligomeric states. Class I FBAs have primarily been characterized as tetrameric species in eukaryotes with a few bacterial class I FBAs forming monomeric to decameric oligomeric states[4]. Previously, only class IIb FBAs were determined to have the same oligomeric range as class I FBAs[4; 21; 22]. The evolutionary pressure for FBAs forming oligomeric structures is currently unknown. However, the prevalence of FBAs forming higher-order oligomeric states, primarily tetramers, coupled with the appearance that these enzymes have independently evolved to form these higher oligomers, suggests an evolutionary advantage for organisms carrying higher oligomeric FBAs.

Reaction mechanism for MtFBA

In contrast to previously determined X-ray structures of class II FBAs in complex with the inhibitor PGH, which only represents an intermediate/analog-state of the substrate DHAP, the X-ray structures of MtFBA reported here represent bona fide substrate, product and intermediate-bound states along the entire reaction pathway. A superposition of the X-ray structures for these complexes is shown in Figure 6. Analysis of these structures, in conjunction with the available literature on site-directed mutagenesis, kinetic and solution biochemical studies for the class II FBAs, has led us to add important structural details to the mechanistic scheme presented in Figure 7 for the reaction catalyzed by these enzymes.

The structure of the MtFBA-DHAP complex helps to provide an understanding of how MtFBA can bind DHAP and carry out its conversion to HEI. Within the MtFBA-DHAP structure, we

observe both DHAP and a molecule with geometry analogous to HEI. The molecules are found bound in a 30:70 ratio of DHAP to HEI. The predominance of an HEI-like intermediate suggests that deprotonation of DHAP occurred prior to or during crystallization. Since MtFBA was first incubated with DHAP at pH 8 before crystallization, deprotonation of DHAP could have occurred during the preincubation period thereby forming HEI (Steps 1 and 2 in Figure 7). Since the enzyme was added to an acidic crystallization solution, solvent derived protons could help stabilize the MtFBA-HEI complex by protonating the enolate oxygen essentially trapping an enediol intermediate (Steps 2 and 3). Unfortunately, it is impossible to distinguish between the two possible intermediates (HEI or an enediol) by X-ray crystallography since they have the same geometry, a problem that neutron diffraction studies could more directly address.

Deprotonation of DHAP during steps 1 and 2 is likely catalyzed by a glutamate residue (E169 in MtFBA). Studies have suggested that a highly conserved glutamate residue located between β5 and α5 (residues 168–180 in MtFBA) is involved in the extraction of the C1 proton from DHAP for class II FBAs (Figure 1)[30]. This loop region is analogous to the well characterized E165 of loop 7 in chicken triose-phosphate isomerase (TIM) responsible for deprotonation of DHAP in TIM. Multiple studies have directly linked increased and decreased flexibility of loop 7 in TIM to a proportional response in k_{cat}[31].

Unfortunately, in all structures of MtFBA, amino acid E169 and the other residues (168–180) within the loop are structurally unresolved. This observation is similar for all other class II FBA structures that have been elucidated. Electron density for the putative catalytic glutamate can only be visualized in the structure of the *E. coli* class IIa FBA in complex with the inhibitor PGH which was formed under a high (2–5 mM) concentration of zinc[25]. In this structure, (PDB: 1B57) the glutamate points toward PGH but is too far away to abstract a proton. However, the position of glutamate may be contorted by the presence of a spurious zinc atom bound near the active site, a zinc not observed in any of the MtFBA structures crystallized in the presence of 0.1 M zinc. Additionally, the position of the loop could be pH dependant as the *E. coli* homolog was crystallized at pH 7.5, instead of MtFBA's pH 4.8. To date, this residue has not been observed in any class II FBA structure to be positioned in a manner that would allow deprotonation of DHAP. However, the presumed proximity of this loop and the associated glutamate to several waters suggests that it may alternatively activate waters via a proton shuttle in the solvent rich, MtFBA active site. At a minimum, the MtFBA-DHAP-G3P and MtFBA-FBP structures assert that the glutamate side chain must be allowed to leave the active site to expose it to solvent and thereby allow G3P or FBP to bind (Figure 6). The inherent flexibility of this loop is critical for the proper deprotonation/protonation and substrate-product binding events which has been demonstrated for Class II FBA from *E. coli*[30] (Figure 7).

The presence of both DHAP and HEI within the active site allows for independent elucidation of their respective interactions with MtFBA. The C1 hydroxyl group of DHAP undergoes H-bonding with active site waters anchored by side chains of D276 and symetry related K308 instead of the side chain of D95 (Figure 3d). Moreover, neither of the oxygen atoms in DHAP is located close enough to the Zn1 to form what would be considered a strong, first-coordination sphere bond. At 2.6 Å, the ketone of DHAP is the closest, but at this distance is more suitably classified as a second sphere H-bond interaction (Figure 3d)[26]. Only upon extraction of the proton from C1 and its conversion to HEI are full coordination bonds observed between the intermediate and MtFBA placing the catalytic zinc in non-ideal trigonal bipyramidal geometry (Figure 3c,d).

In addition to the required movement of the glutamate out of the active site so that G3P can bind, the coordination state of the catalytic zinc changes upon G3P binding The active site structure of the MtFBA-DHAP-G3P complex shows that only the C1 hydroxyl oxygen

maintains a short bond distance ~ 2.2 Å with the Zn1 cation. The C2 oxygen bond distance of HEI to Zn1 increases to 2.6 Å (Figure 4c). This suggests that the electronic nature surround the C2 ketone or hydroxyl (enediol) may change after proton extraction from C1 and subsequent binding of G3P..

The MtFBA-G3P-DHAP/HEI structure also adds clarity to step IV of the reaction mechanism (Figures 6 and 7). Previous studies have proposed an interaction between the aldehyde on G3P with D95 (MtFBA residue number) in the DHAP-G3P complex prior to catalysis[25; 30; 32]. The X-ray structures of the MtFBA-DHAP-G3P and MtFBA-HEI-G3P complexes add important new details to this part of the catalytic reaction. The structure of the MtFBA-DHAP-G3P complex shows that prior to catalysis, this bond has not yet formed since the G3P ketone is incorrectly oriented to create this interaction (Figure 4). Analysis of the MtFBA-HEI-G3P structure suggests that during the formation of this complex, a significant movement of the ketone oxygen occurs during the condensation reaction so that D95 can interact with the oxygen and thereby protonate the developing negative charge (Figure 7). In addition, the MtFBA-FBP structure illustrates that the resulting hydroxyl (C4 on FBP or C1 from G3P) forms a coordination bond with the Zn1 suggesting that the zinc atom serves to activate G3P in addition to D95 (Figures 5 and 6).

Finally, by comparing the MtFBA-G3P-DHAP and MtFBA-FBP active sites, the formation of the C3 and C4 bond of FBP during the condensation step of the reaction can be envisioned. The C1 of G3P moves within 3.3 Å of the C1 of HEI before catalysis while simultaneously rotating the oxygen of the aldehyde of G3P towards the zinc atom (Figure 5c). Upon formation of FBP, the C2, C3 and C4 oxygen atoms all coordinate to the zinc atom, although to varying extents (Figure 7), and the C4 hydroxyl oxygen comes within hydrogen bonding distance of D95. This latter residue has been shown via site directed mutagenesis studies to be critical for deprotonation of FBP in the forward/glycolytic reaction direction[30; 32].

Specificity of Class I and Class II FBAs for FBP

In addition to clarifying the final steps of the FBA mechanism, the MtFBA-FBP structure also provides information for future structure based design endeavors aimed at inhibiting class II FBAs. The conformation that FBP adopts when bound to MtFBA is divergent to those observed in class I FBA structures. When MtFBA-FBP is aligned via Secondary Structure Matching (SSM) with human aldolase complexed with FBP, the conformational differences become clear (Figure 8)[33]. When bound to MtFBA, FBP adopts a more constrained orientation where the hydroxyls of C3, C4 and the ketone of C2 point towards the zinc ion forming coordination bonds. In the human class I FBA structure, only two hydroxyls on C3 and C4, face themselves in the same direction with the C2 ketone which is oriented in the opposite direction (Figure 8). Small molecules designed to exploit the conformational differences of FBP between classes I and II FBAs could enhance selectivity.

In conclusion, the structures of MtFBA bound to DHAP/HEI, DHAP-G3P, and FBP, provide new and valuable information towards our understanding of the class II FBA reaction mechanism and subunit association of class IIa FBAs thereby providing greater predictability of FBA oligomeric states across species in general. The structures of MtFBA and the structures of the human class I FBAs should now provide a basis for structure based inhibitor design studies aimed at selectively targeting FBA from *M. tuberculosis.*

Materials and Methods

Construction of MtFBA expression vectors

The *M. tuberculosis fba* gene (Rv0363c) was PCR-amplified from *M. tuberculosis* H_{37}RV genomic DNA using the oligonucleotides 5′-GGTGGT**CATATG**CCTATCGCAACGCCC -3′ and 5′-GA**AGATCT**AATGGTGATGGTGATG GTGGGTTAGGGACTTTC -3′ as the forward and the reverse primers, respectively. *Nde*I and *Bgl*II restriction sites (in bold) were incorporated into the two primers. Five histidine codons were also added into the reverse primer. The PCR product was cleaned by the QIAquick PCR purification kit (Qiagen) and digested with *Nde*I and *Bgl*II enzymes. The digested fragment was purified and cloned into the expression vector pET17b using *Nde*I and *BamH*I ends to form the pET-fbaH construct, which produces a C-terminal His-tagged fusion protein referred to at MtFBA. The construct was introduced into *E. coli* BL21(DE3) cells by heat-shock transformation. Then the resulting pET-fbaH plasmid was purified, restriction analyzed and sequenced to verify the construct.

Production and purification of of MtFBA

E. coli harboring pET-fbaH was grown at 37 °C in 8-L of LB broth containing 100 μg/mL of ampicillin until the OD_{600} was about 0.6 and then induced by 0.4 mM IPTG. The culture was further grown for 4–6 h at 25 °C and then centrifuged at 3000×g for 15 min. Cells were washed with PBS and stored at −20 °C until use. The cell pellets collected from 8-L culture were lysed by the addition of BugBuster Master Mix (Novagen) following manufacturer's instructions. Insoluble cell debris was removed by centrifugation at 16,000×g for 20 min at room temperature. The clarified extract was loaded directly onto Ni-NTA Bind Resin (Novagen) pre-equilibrated in buffer A (50 mM sodium phosphate buffer pH 8.0 and 300 mM NaCl) with 10 mM imidazole. MtFBA bound to the Ni-NTA column that then was washed with 32 column volumes of buffer A plus 20 mM imidazole followed by 40 column volumes of buffer A plus 50 mM imidazole. MtFBA was eluted from the column with 6 column volumes of buffer A plus 250 mM imidazole. The eluate was subsequently concentrated in a Amicon-15 Ultracel-100K (Millipore) centrifuge concentrator and dialyzed against an exchange buffer (20 mM Tricine buffer pH 8, 100 mM NaCl, 0.1 mM $ZnCl_2$ and 2mM DTT) prior to application to a gel-filtration.

MtFBA was applied to a Superdex-200 Hiload 26/60 FPLC column pre-equilibrated with the exchange buffer and eluted at a flow rate of 4 mL/min. Fractions were pooled according to the chromatogram, concentrated to 12 mg/mL in an Amicon-15 Ultracel-100K (Millipore) centrifuge concentrator and filtered through 0.65 μm membrane filter. Approximately, 80 mg of protein was obtained from 8 liters of culture medium.

MtFBA Crystallization

Initial crystal conditions for MtFBA were determined from high-throughput screening of Qiagen Nextel Screens, Classics, Classics II, PEGs, PEGs II, Anion, Cation, PhClear I, and PhClear II suites, in a 96 well sitting drop format using a Tecan Freedom Evo 200 liquid handling robot. Drops were 1 μL protein solution to 1 μL precipitate with a 100 μL reservoir volume. Samples of 12 mg/mL protein solutions in 20 mM Tricine buffer pH 8, 100 mM NaCl, 0.1 mM $ZnCl_2$ and 2mM DTT were used for the screening. Initial screening resulted in several hits, all in conditions containing high PEGs with weights greater than 3350 and pH above 7.5. Crystals resulting from these conditions appeared to be bipyramidal in morphology and proved to provide poor diffraction (data not shown).

Subsequently, a second screen, using the same 768 conditions and protein concentration, was conducted with MtFBA in the presence of 270 μM of either DHAP (Sigma D7137) or FBP (Sigma F0752) added to the protein solution prior to crystallization. Results of this screen

largely mirrored that of the apo screen but had a few additional hits. Analysis of these additional hits revealed one condition that formed MtFBA crystals that were cubic in morphology and formed in a relatively divergent condition, 30% PEG 300 and 0.1 M NaAcetate pH 4.8. Final crystals for all structures were obtained by vapor diffusion with 500 μL reservoir 4 μL hanging drops mixed 1:1 with protein solution and precipitant, 26% PEG 300 and 0.1 M NaAcetate pH 4.8. Co-crystals for MtFBA-DHAP complex were sourced from drops in which the MtFBA protein solution containing 270 μM DHAP was used. MtFBA-1,6 fructose bisphosphate complex crystals were sourced from crystals co-crystallized in the presence of protein solution containing 270 μM FBP then soaked in mother liquor containing 2 mM 1,6 fructose bisphosphate for 24 hrs. MtFBA-DHAP-G3P complex crystals were derived from crystals generated by co-crystallization of MtFBA-DHAP and soaked with 2 mM G3P (Sigma G5251) for 24 hrs.

X-ray Structural Determination of MtFBA DHAP, DHAP-G3P and FBP Complexes

The X-ray data set for MtFBA-DHAP-G3P was collected on our in house, HR200 Rigaku rotating copper anode source using a 1.54 Å wavelength X-ray beam. X-ray data sets for MtFBA-DHAP and MtFBA-FBP were collected at SER-CAT beamline 22-BM and 22-ID respectively. All crystals were mounted on nylon loops and submerged in a 5 μL cryo solution of 30% PEG 300 and 0.1 M NaAcetate pH 4.8. Crystals were subsequently flash frozen in liquid nitrogen. Frozen crystals were mounted under stream of dry N_2 at 100°K. All datasets were collected using 0.5 degree oscillations using either an area RAXIS IV^{++} detector (MtFBA-DHAP-G3P) or CCD detectors, MAR 225 (MtFBA-DHAP) and MAR 300 (MtFBA-FBP) X-ray images were indexed, processed, integrated and scaled together using the program HKL2000[34].

A molecular replacement solution for MtFBA-DHAP was obtained using the CCP4 suite and the molecular replacement tool Phaser with a 3D-JIGSAW, homology protomer model of MtFBA based on *E. coli* FBA (1B57)[35; 36]. WinCoot was used for model building, and Refmac5.2 from the CCP4 suite used for refinement[36]. Coordinates and molecular library files for the ligands DHAP, G3P, HEI and FBP were built using the program CCP4 suite program Sketcher. Final refinement was conducted using translation libration screw (TLS) restraints from TLS motion determination[37]. Isotropic temperature factors were refined for the MtFBA-DHAP and MtFBA-DHAP-G3P structures, whereas anisotropic temperature factors were used for the MtFBA-FBP. Water molecules were added to F_o-F_c density peaks that were greater than 3σ using the "Find Water" winCoot program function. The final models were checked for structural quality using the CCP4 suite programs, Procheck and Sfcheck.

Acknowledgements

This research was supported in part by grants from the National Institutes of Health Grant P01AI060915 (SDP, ADM), Department of Defense Grant W81XWH0710445 USAMRAA (ADM) and National Center for Genetic Engineering and Biotechnology, Thailand (KR). Data were collected at Southeast Regional Collaborative Access Team (SER-CAT) 22-ID and 22-BM beamlines at the Advanced Photon Source, Argonne National Laboratory. Supporting institutions may be found at www.ser-cat.org/members.html. Use of the Advanced Photon Source was supported by the U. S. Department of Energy, Office of Science, Office of Basic Energy Sciences, under Contract No. W-31-109-Eng-38.

References

1. World Health Organization. Global tuberculossis control -surveillance, planning, financing. 2008
2. World Health Organization. Tuberculosis MDR-TB & XDR-TB. 2008 February;
3. Rutter WJ. Evolution of Aldolase. Fed Proc 1964;23:1248–57. [PubMed: 14236133]

4. Ramsaywak PC, Labbe G, Siemann S, Dmitrienko GI, Guillemette JG. Molecular cloning, expression, purification, and characterization of fructose 1,6-bisphosphate aldolase from Mycobacterium tuberculosis--a novel Class II A tetramer. Protein Expr Purif 2004;37:220–8. [PubMed: 15294302]
5. Izard T, Sygusch J. Induced fit movements and metal cofactor selectivity of class II aldolases: structure of Thermus aquaticus fructose-1,6-bisphosphate aldolase. J Biol Chem 2004;279:11825–33. [PubMed: 14699122]
6. Galkin A, Kulakova L, Melamud E, Li L, Wu C, Mariano P, Dunaway-Mariano D, Nash TE, Herzberg O. Characterization, kinetics, and crystal structures of fructose-1,6-bisphosphate aldolase from the human parasite, Giardia lamblia. J Biol Chem 2007;282:4859–67. [PubMed: 17166851]
7. Marsh JJ, Lebherz HG. Fructose-bisphosphate aldolases: an evolutionary history. Trends Biochem Sci 1992;17:110–3. [PubMed: 1412694]
8. Gerdes SY, Scholle MD, Campbell JW, Balazsi G, Ravasz E, Daugherty MD, Somera AL, Kyrpides NC, Anderson I, Gelfand MS, Bhattacharya A, Kapatral V, D'Souza M, Baev MV, Grechkin Y, Mseeh F, Fonstein MY, Overbeek R, Barabasi AL, Oltvai ZN, Osterman AL. Experimental determination and system level analysis of essential genes in Escherichia coli MG1655. J Bacteriol 2003;185:5673–84. [PubMed: 13129938]
9. Stribling D, Perham RN. Purification and characterization of two fructose diphosphate aldolases from Escherichia coli (Crookes' strain). Biochem J 1973;131:833–41. [PubMed: 4198624]
10. Baba T, Ara T, Hasegawa M, Takai Y, Okumura Y, Baba M, Datsenko KA, Tomita M, Wanner BL, Mori H. Construction of Escherichia coli K-12 in-frame, single-gene knockout mutants: the Keio collection. Mol Syst Biol 2006;2:2006–0008.
11. Scamuffa MD, Caprioli RM. Comparison of the mechanisms of two distinct aldolases from Escherichia coli grown on gluconeogenic substrates. Biochim Biophys Acta 1980;614:583–90. [PubMed: 6996735]
12. Davis EO, Jones-Mortimer MC, Henderson PJ. Location of a structural gene for xylose-H+ symport at 91 min on the linkage map of Escherichia coli K12. J Biol Chem 1984;259:1520–5. [PubMed: 6363412]
13. Rosenkrands I, Slayden RA, Crawford J, Aagaard C, Barry CE 3rd, Andersen P. Hypoxic response of Mycobacterium tuberculosis studied by metabolic labeling and proteome analysis of cellular and extracellular proteins. J Bacteriol 2002;184:3485–91. [PubMed: 12057942]
14. Bai NJ, Pai MR, Murthy PS, Venkitasubramanian TA. Effect of oxygen tension on the aldolases of Mycobacterium tuberculosis H37Rv. FEBS Lett 1974;45:68–70. [PubMed: 4213059]
15. Rukseree, K. PhD Dissertation. Mahidol Uiversity; 2007. Fructose-1,6-biphosphate aldolase as a potential drug target for tuberculosis.
16. Zhang Y. The magic bullets and tuberculosis drug targets. Annu Rev Pharmacol Toxicol 2005;45:529–64. [PubMed: 15822188]
17. Fonvielle M, Weber P, Dabkowska K, Therisod M. New highly selective inhibitors of class II fructose-1,6-bisphosphate aldolases. Bioorg Med Chem Lett 2004;14:2923–6. [PubMed: 15125960]
18. Gavalda S, Braga R, Dax C, Vigroux A, Blonski C. N-Sulfonyl hydroxamate derivatives as inhibitors of class II fructose-1,6-diphosphate aldolase. Bioorg Med Chem Lett 2005;15:5375–7. [PubMed: 16236509]
19. Nakahara K, Yamamoto H, Miyake C, Yokota A. Purification and characterization of class-I and class-II fructose-1,6-bisphosphate aldolases from the cyanobacterium Synechocystis sp. PCC 6803. Plant Cell Physiol 2003;44:326–33. [PubMed: 12668779]
20. Plaumann M, Pelzer-Reith B, Martin WF, Schnarrenberger C. Multiple recruitment of class-I aldolase to chloroplasts and eubacterial origin of eukaryotic class-II aldolases revealed by cDNAs from Euglena gracilis. Curr Genet 1997;31:430–8. [PubMed: 9162115]
21. Sauve V, Sygusch J. Molecular cloning, expression, purification, and characterization of fructose-1,6-bisphosphate aldolase from Thermus aquaticus. Protein Expr Purif 2001;21:293–302. [PubMed: 11237691]
22. Cooper SJ, Leonard GA, McSweeney SM, Thompson AW, Naismith JH, Qamar S, Plater A, Berry A, Hunter WN. The crystal structure of a class II fructose-1,6-bisphosphate aldolase shows a novel binuclear metal-binding active site embedded in a familiar fold. Structure 1996;4:1303–15. [PubMed: 8939754]

23. Janin J, Miller S, Chothia C. Surface, subunit interfaces and interior of oligomeric proteins. J Mol Biol 1988;204:155–64. [PubMed: 3216390]
24. Krissinel E, Henrick K. Inference of macromolecular assemblies from crystalline state. J Mol Biol 2007;372:774–97. [PubMed: 17681537]
25. Hall DR, Leonard GA, Reed CD, Watt CI, Berry A, Hunter WN. The crystal structure of Escherichia coli class II fructose-1, 6-bisphosphate aldolase in complex with phosphoglycolohydroxamate reveals details of mechanism and specificity. J Mol Biol 1999;287:383–94. [PubMed: 10080900]
26. Alberts IL, Nadassy K, Wodak SJ. Analysis of zinc binding sites in protein crystal structures. Protein Sci 1998;7:1700–16. [PubMed: 10082367]
27. Qamar S, Marsh K, Berry A. Identification of arginine 331 as an important active site residue in the class II fructose-1,6-bisphosphate aldolase of Escherichia coli. Protein Sci 1996;5:154–61. [PubMed: 8771208]
28. Zgiby SM, Thomson GJ, Qamar S, Berry A. Exploring substrate binding and discrimination in fructose1, 6-bisphosphate and tagatose 1,6-bisphosphate aldolases. Eur J Biochem 2000;267:1858–68. [PubMed: 10712619]
29. May M, Mehboob S, Mulhearn DC, Wang Z, Yu H, Thatcher GR, Santarsiero BD, Johnson ME, Mesecar AD. Structural and functional analysis of two glutamate racemase isozymes from Bacillus anthracis and implications for inhibitor design. J Mol Biol 2007;371:1219–37. [PubMed: 17610893]
30. Zgiby S, Plater AR, Bates MA, Thomson GJ, Berry A. A functional role for a flexible loop containing Glu182 in the class II fructose-1,6-bisphosphate aldolase from Escherichia coli. J Mol Biol 2002;315:131–40. [PubMed: 11779234]
31. Thanki N, Zeelen JP, Mathieu M, Jaenicke R, Abagyan RA, Wierenga RK, Schliebs W. Protein engineering with monomeric triosephosphate isomerase (monoTIM): the modelling and structure verification of a seven-residue loop. Protein Eng 1997;10:159–67. [PubMed: 9089815]
32. Plater AR, Zgiby SM, Thomson GJ, Qamar S, Wharton CW, Berry A. Conserved residues in the mechanism of the E. coli Class II FBP-aldolase. J Mol Biol 1999;285:843–55. [PubMed: 9878448]
33. Dalby A, Dauter Z, Littlechild JA. Crystal structure of human muscle aldolase complexed with fructose 1,6-bisphosphate: mechanistic implications. Protein Sci 1999;8:291–7. [PubMed: 10048322]
34. Otwinowski, Z.; Minor, W. Processing of X-ray Diffraction Data Collected in Oscillation Mode. In: Carter, CW.; Sweet, RM., editors. Methods in Enzymology, Macromolecular Crystallography, Part A. Vol. 276. Academic Press; New York: 1997.
35. Bates PA, Kelley LA, MacCallum RM, Sternberg MJ. Enhancement of protein modeling by human intervention in applying the automatic programs 3D-JIGSAW and 3D-PSSM. Proteins 2001;(Suppl 5):39–46. [PubMed: 11835480]
36. The CCP4 suite: programs for protein crystallography. Acta Crystallogr D Biol Crystallogr 1994;50:760–3. [PubMed: 15299374]
37. Painter J, Merritt EA. Optimal description of a protein structure in terms of multiple groups undergoing TLS motion. Acta Crystallogr D Biol Crystallogr 2006;62:439–50. [PubMed: 16552146]

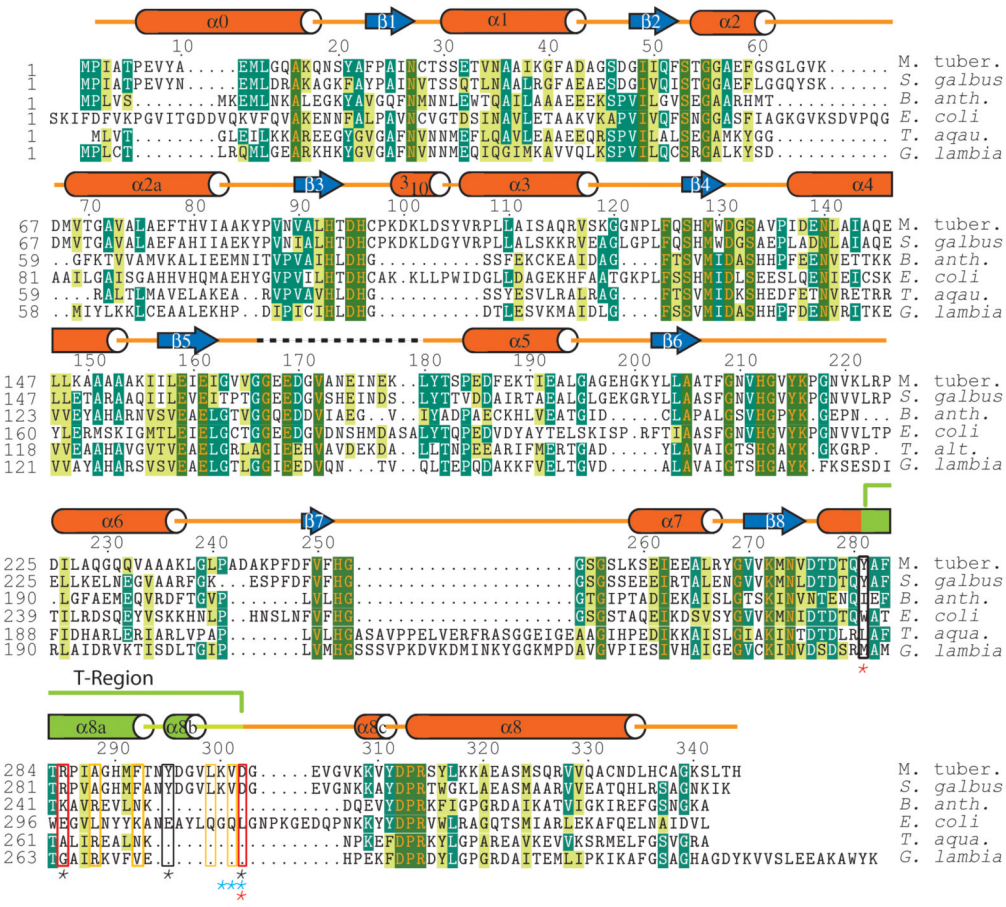

Figure 1. Sequence alignment of various FBP aldolases

FBAs are from H37RV strain of *M. tuberculosis* (protein accession NP_334786), *S. galbus* (protein accession CAA10483), *B. anthracis* (protein accession NP_847736), *E. coli* (PDB 1B57_A), *T. aquaticus* (PDB 1RV8_A), *G. lambia* (PDB 2ISV_A). The alignment was generated using CLUSTALW, TEXSHADE, and BL2SEQ programs (http://workbench.sdsc.edu/) were used with the Matrix = BLOSUM62, Gap Opening Penalty = 11, Gap Extension Penalty = 1, and Lambda Ratio = 0.85. Amino acids are color coded according to being non-conserved (white), similiar (lime green), conserved (green), and completely conserved (dark green; orange lettering) across the six sequences. Secondary structure of MtFBP aldolase according to Defined Secondary Structure of Proteins (DSSP) is represented in orange cylinders (helical regions), blue arrows (β-sheet regions), loops (yellow-orange), T-region (green) and dashed-lines (missing residues). Residues in the T-region are bracketed according to type of tetrameric interactions they form. Residue side-chain properties are colored according charge (red), hydrophobicity (yellow), or both (black). Red and black asterisks indicate interaction partners while cyan asterisks indicate backbone H-bond interactions.

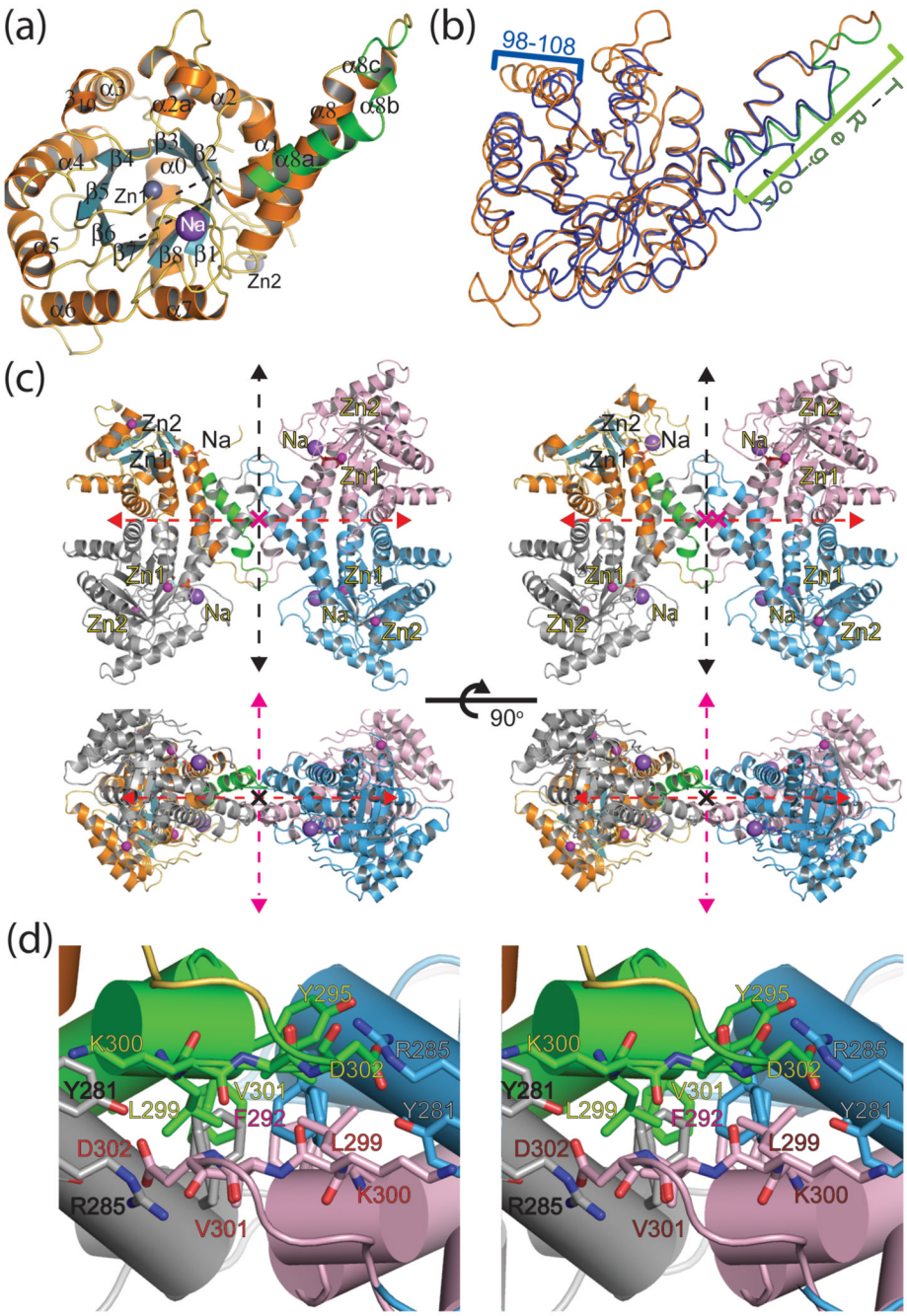

Figure 2. Overall monomer and tetramer structures of MtFBP aldolase illustrating the unique tetramerization interface of Class IIa FBAs

(a) Cartoon representation of the MtFBP protomer bound with DHAP. Helical regions are rendered in orange, beta strands in light blue, and loops in yellow-orange. Zinc (grey) and sodium (purple) are illustrated as spheres. Missing residues 168–180 represented by dashed lines. **(b)** Structure of a tetrameric class II 1,6 fructose bisphosphate aldolase Secondary Structure Matching alignment of MtFBA (orange) with chain A of FBA from *T. aquaticus* (PDB 1RV8_A; blue). T-region of MtFBA is colored in green. **(c)** Tetramer of MT-FBP with asymmetric unit protomer colored according to (A) with T-region highlighted in green. Symmetry related protomers in pink, grey, and light blue with sodium (purple) and zinc (hot

pink) depicted as spheres. DHAP and HEI is present in light cyan. Three axis are present (red, black, magenta) illustrate crystallographic symmetry planes. Labels are in black for a one protomer and in yellow for one of its symmetry related protomers. **(d)** Close up of the T-region rendered with residues represented as sticks and colored as in (c). Labels are in orange for protomer residues and outlined for symmetry related residues.

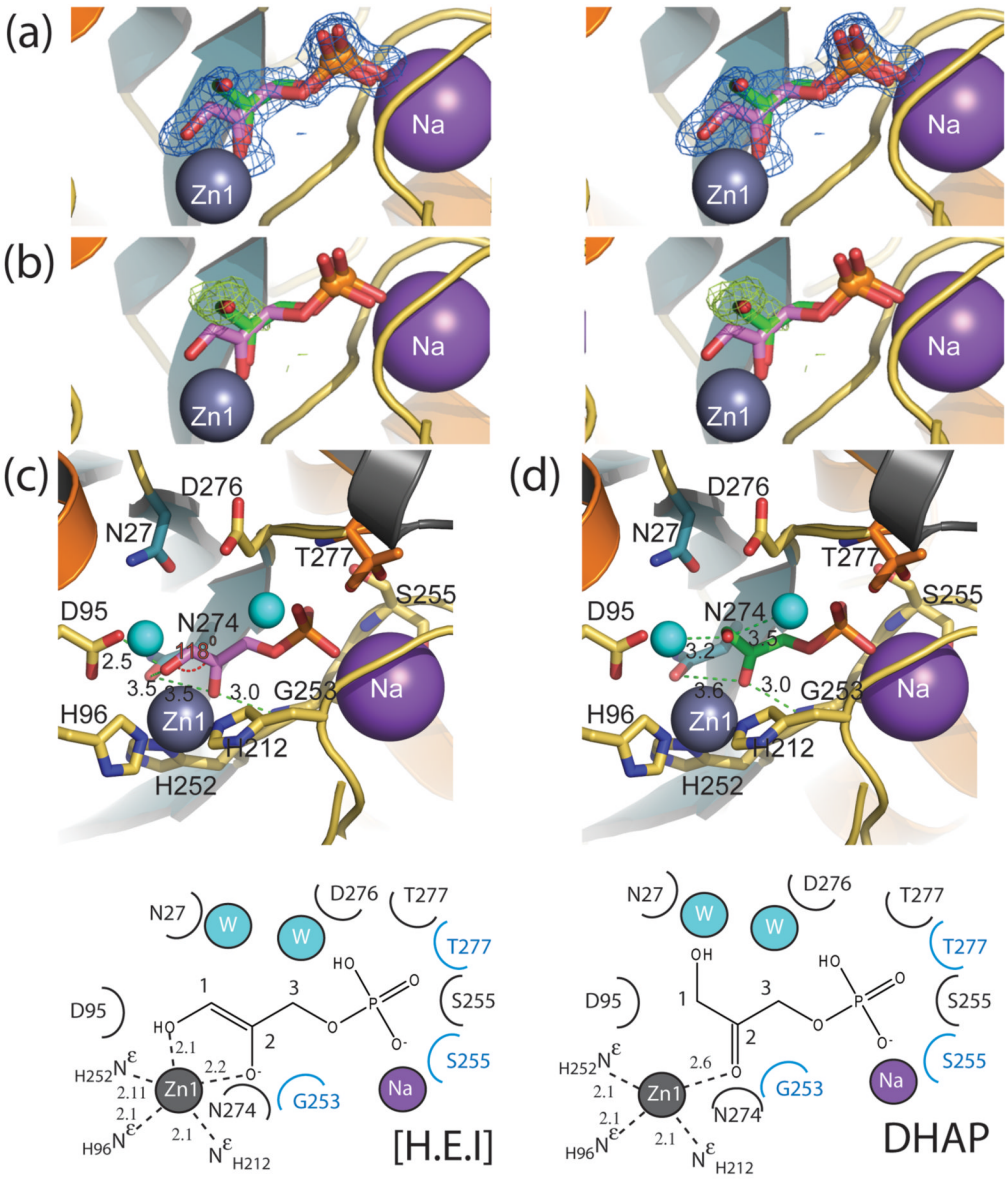

Figure 3. Active site structure of the MtFBA-DHAP complex

(a) Divergent-eyed stereo view of MtFBA active site with DHAP (green) and reaction intermediate HEI (violet). Asymmetric protomer carbons are colored according to secondary structure, orange (helix), yellow-orange (loop) and dark cyan (β-strand). Heteroatoms are colored according to their element. Zinc (grey) and sodium (purple) ions are rendered in sphere according to atomic size. The $2F_o$-F_c density maps calculated with with DHAP and HEI present are contoured (blue) at 1 σ. **(b)** F_o-F_c electron density maps, calculated without DHAP present, are contoured (green) at 3σ. Colors for residues, ions, DHAP, and HEI are the same as in (a). **(c)** The active site of the MtFBA-DHAP complex, with DHAP removed for clarity, is shown in the top panel. Symmetry related monomer cartoon is depicted in gray. Angles and associated labels are colored red with distances and associated labels colored green. Water molecules (cyan) are depicted as spheres and are Structure of a tetrameric class II 1,6 fructose bisphosphate aldolase scaled to 50% for clarity. All other colors are as in (a). A 2-Dimensional representation of HEI bound to MtFBA with is shown in the bottom panel. Residue labels and

crescents are colored in black and illustrate the interaction of residues with HEI mediated through their side chains. Residue labels and crescents colored in cyan represent residues interacting with HEI through backbone heteroatoms. **(d)** The active site of the MtFBA-DHAP complex, with HEI removed for clarity, is shown in the top panel. Lines and associated labels for distance and are in green. Water molecules (cyan) are depicted as spheres and are scaled to 50% for clarity. All other colors are as in (a). A 2-dimensional representation of DHAP bound to MtFBA is shown in the bottom panel. Residue labels and crescents in black illustrate interaction of residues with HEI mediated through their side chains. All colors are as in (c).

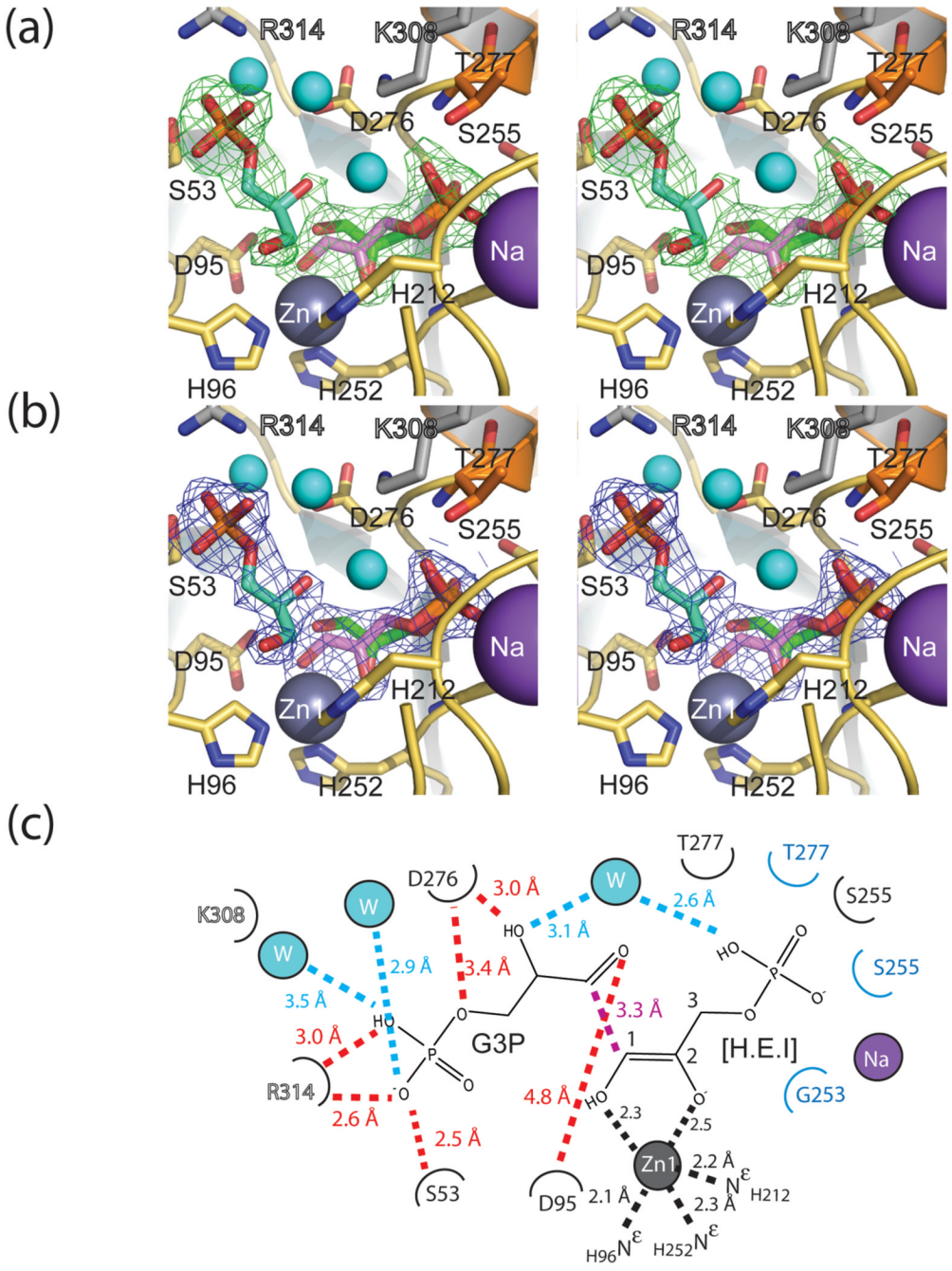

Figure 4. X-ray structure of the MtFBA-DHAP-G3P complex

(a) Divergent-eyed stereo view of the MtFBA active site with the substrate DHAP (green), the reaction intermediate HEI (violet), and substrate G3P (teal). Carbons are colored according to their location in secondary structure; orange (helix), yellow-orange (loop) and dark cyan (β-strand). The carbons of the symmetry related monomer are depicted in grey. Heteroatoms are colored according to their element. Waters molecules (cyan) are depicted as spheres and are scaled to 50% for clarity. Zinc (grey) and sodium (purple) ions are rendered as spheres according to atomic size. The F_o-F_c electron density maps are calculated without DHAP, HEI, or G3P, and are contoured (green) at 3σ. **(b)** Divergent-eyed stereo view of the MtFBA active site as in (a) but with a $2F_o$-F_c electron density map (blue) calculated at 1σ and surrounding

DHAP, HEI, and G3P. Only density Structure of a tetrameric class II 1,6 fructose bisphosphate aldolase close to the ligands is shown for clarity. **(c)** 2-dimensional representation of the active site surrounding G3P and HEI. Residue colors and labels indicate interactions formed by one monomer (black), and its symmetry related monomer (outlined). Other labels are colored according to the substrate they are derived from. Residues of MtFBA interacting with HEI are removed for clarity.

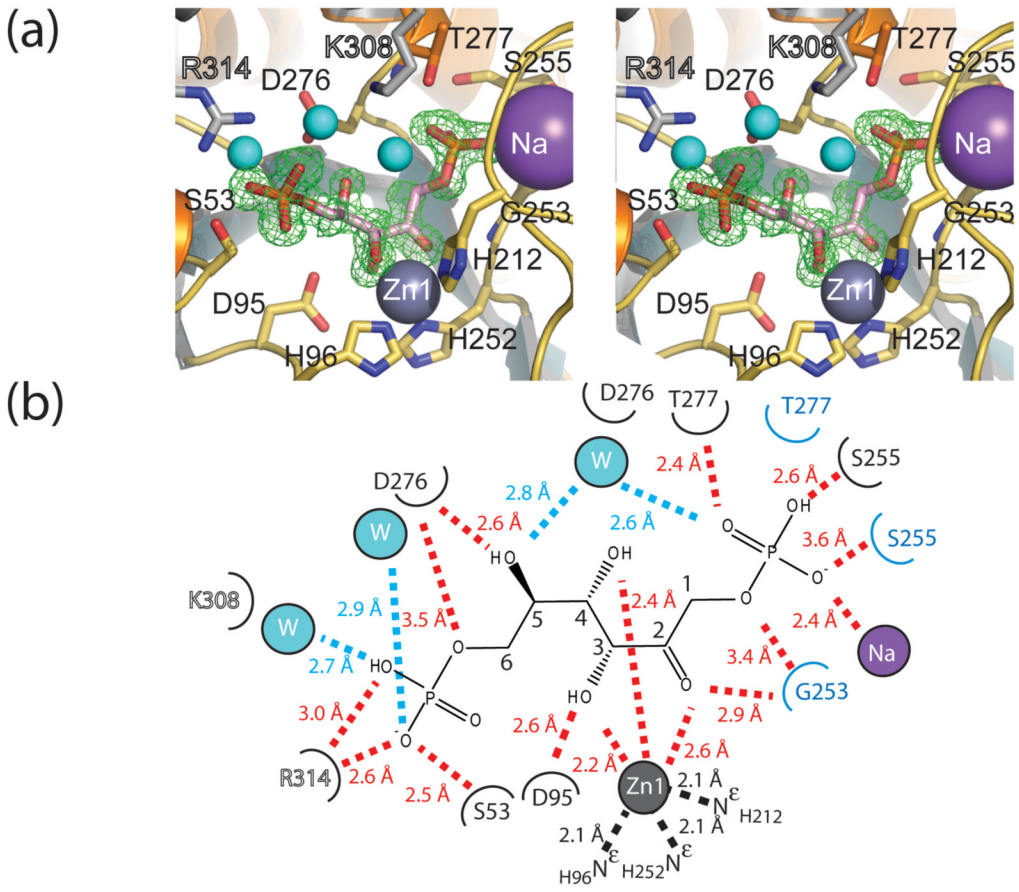

Figure 5. X-ray structure of the MtFBA active site with FBP bound

(a) Divergent-eyed stereo view of the MtFBA-FBP active site. Residues are colored according to secondary structure, orange (helix), dark cyan (β-strand), and yellow-orange (loop). Symmetrically related monomers are depicted in grey. All heteroatoms are colored according to their respective elemental colors. Water molecules (cyan), zinc (grey), and sodium (purple) are rendered as spheres. Zinc and sodium are scaled to their atomic radii with waters at 50% scaling for clarity. The F_o-F_c electron density map (green) is calculated in the absence of fructose-1,6- bisphosphate and is contoured at 3σ. **(b)** 2-dimensional illustration of the active site surrounding FBP. Monomer residues are in solid black labels and symmetry related monomer residues have outlined black labels.

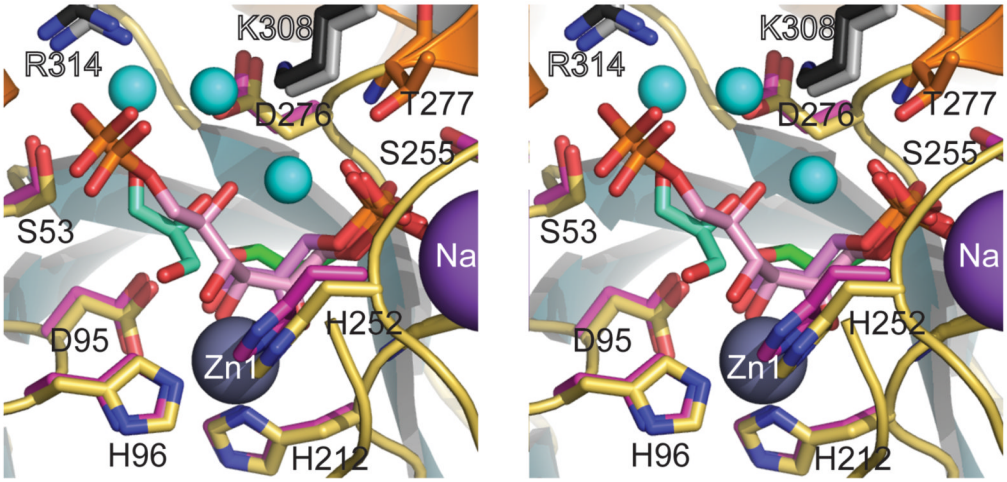

Figure 6. Divergent-eyed stereo view of a superposition of the MtFBA-FBP and MtFBA-DHAP-G3P complexes

Residues of MtFBA-FBP are colored according to their secondary structure location; orange (helix), dark cyan (β-strand), and yellow-orange (loop). Symmetrically related monomers are depicted in grey. All heteroatoms are colored according to their respective elemental colors. Waters (cyan), zinc (grey), and sodium (purple) are rendered as spheres. Zinc and sodium are scaled to their atomic Structure of a tetrameric class II 1,6 fructose bisphosphate aldolase radii with waters at 50% scaling for clarity. The MtFBA-DHAP-G3P structure is represented in magenta with symmetry related monomer in dark grey.

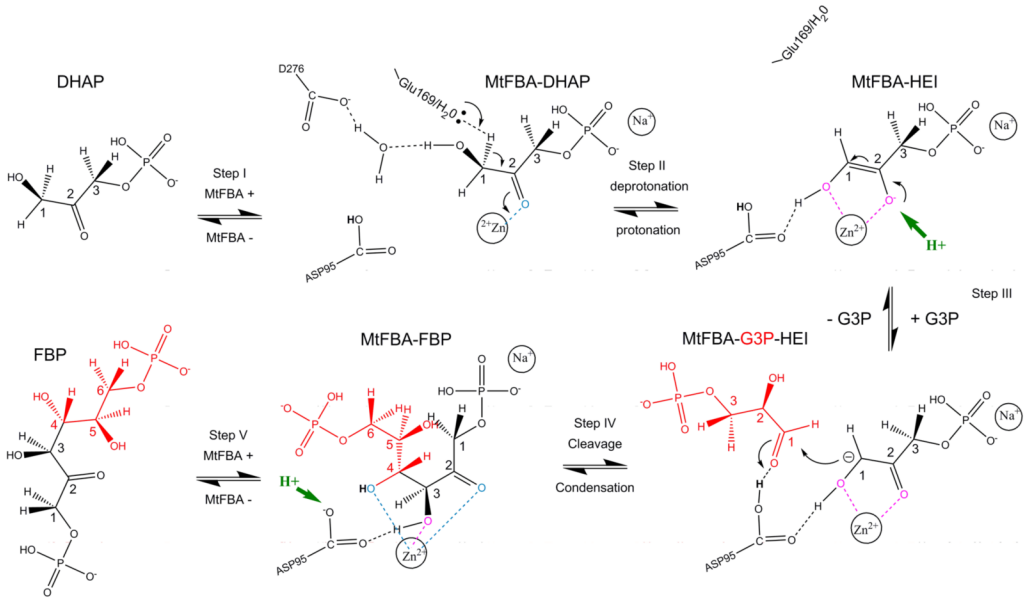

Figure 7. Proposed reaction mechanism for MtFBA

with elements sourced from G3P in red. Blue and magenta denote coordination and H-bonds formed with the Zn1 respectively. Green highlights places in the mechanism that proton trapping could occur.

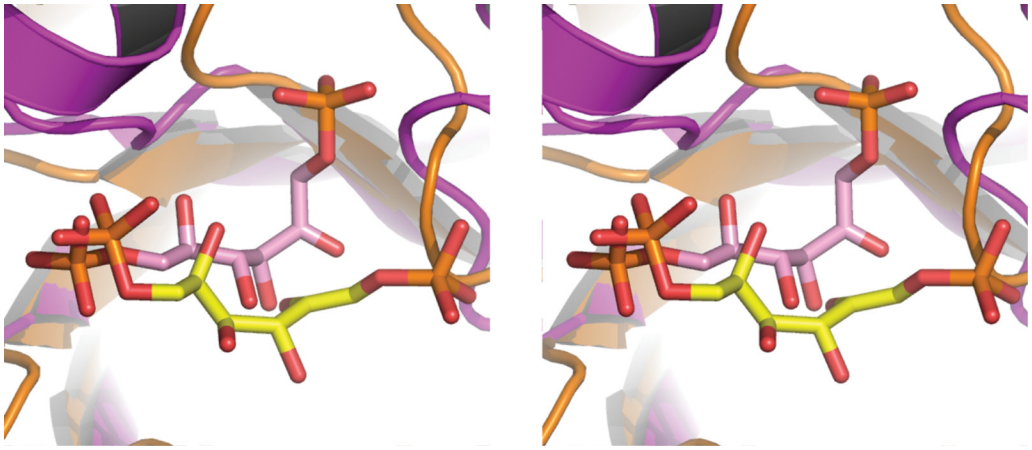

Figure 8. Different binding orientations for FBP to Class I and Class II FBAs

A stereoview of the MtFBA-FBP active site is shown superposed with human muscle aldolase bound with FBP (4ALD). The MtFBA-FBP structure is colored orange with FBP colored pink. Human aldolase is in shown in purple with the bound FBP molecule colored yellow. The Zn1and Na molecules have been removed from the MtFBP active site for clarity.

Table 1
Data Collection and Refinement

	MtFBA-DHAP	MtFBA-DHAP-G3P	MtFBA-FBP
Data Collection			
Space Group	I222	I222	I222
Unit Cell Dimensions			
a, b, c (Å)	61.3, 120.2, 164.8	61.2, 120.5, 164.3	60.6, 119.5, 164.0
α=β =γ (°)	90.0	90.0	90.0
Resolution (Å)	97.1–1.5	97.1–2.1	96.7–1.3
No. Reflections Observed	421,305	105,670	688,310
No. Unique Reflections	91,761	36,655	140,514
R_{merge} (%)[a]	5.4 (21.1)*	5.0 (9.0)*	5.8 (31.3)*
I/σI	21.4 (4.6)*	14.7 (10.6)*	26.4 (4.1)*
% Completeness	96.5 (89.6)*	91.4 (78.5)*	98.9 (94.8)*
Refinement			
Resolution Range	97.1–1.5	97.1–2.1	96.7–1.3
No. Reflections in Working Set	87,153	34,810	133,473
No. Reflections in Test Set	4,602	1,592	7,033
R_{work} (%)[b]	16.7	15.8	15.8
R_{free} (%)[b]	17.8	18.1	17.0
RMS deviation:			
Bond Lengths (Å)	0.01	0.02	0.01
Bond Angles (°)	0.73	1.74	1.20
Protein/Water Atoms	3274/533	2985/365	3257/533
Average B-Factors (Å^2)	3274/533	2985/365	3257/533
Total	22.6	25.2	20.8
Protein	19.8	18.6	18.4
Water	34.6	34.6	41.0
Ligands	20.6	24.9	17.2
Ions	17.5	26.0	15.0

*The last resolution shell is shown in parentheses.

[a] $R_{merge}=\Sigma_h\Sigma_I |I_I(h) - <I(h)>|/\Sigma_h\Sigma_i I_I(h)$, where $I_I(h)$ is the i^{th} measurement and $<I(h)>$ is the weighted mean of all measurements of I(*h*).

[b] R_{work} and $R_{free} = h(|F(h)_{obs}| - |F(h)_{calc}|)/h|F(h)_{obs}|$ for reflections in the working and test sets, respectively. R.m.s., root mean square.